Dewen et al., *Cogent Engineering* (2018), 5: 1482589
https://doi.org/10.1080/23311916.2018.1482589

cogent engineering

MECHANICAL ENGINEERING | RESEARCH ARTICLE

Finite element simulation of high-speed finish milling of SKD11 hardened steel based on modified constitutive equation

Tang Dewen[1,2*], Peng Cong[2] and Zhang Jiayu[2]

Received: 16 February 2018
Accepted: 20 May 2018
First Published: 28 June 2018

*Corresponding author: Tang Dewen, School of mechanical engineering, University of South China, Hunan, Hengyang, 421001
E-mail: will998@163.com

Reviewing editor:
Rubina Bahar, International Islamic University Malaysia, Malaysia

Additional information is available at the end of the article

Abstract: High precision parts have been widely used in automobile, aerospace, medical and other fields. Conventional machining methods are difficult to meet the requirements of the high-quality requirements of components, including shape precision, dimensional accuracy, surface finish and surface integrity. Using milling instead of grinding can significantly improve machining efficiency of ultra-precision parts for difficult cut materials, especially high hardness SKD11 hardened steel. To improve the surface quality and the processing surface integrity of the parts, high-speed milling (HSM) can be able to meet the high-quality requirements of components. However, the quality of finish HSM is difficult to control through experiments. Therefore, the modified flow stress model of SKD11 hardened steel based on SHPB experimental is adopted to simulate the high-speed finish milling in this paper. The effect of cutting parameters on chip formation, cutting temperature, stress and cutting force of SKD11 are analyzed. Compared with the experimental data of cutting force of different cutting parameters, the simulation results are the same as the measured data. The results show that the model can predict the performance of the SKD11 high-speed finish milling process accurately.

Tang Dewen

ABOUT THE AUTHORS

Tang Dewen, male, was born in 1976, PhD, associate professor, associate dean of mechanical engineering school, University of South China, in China. My current research focuses on advanced manufacturing technology and equipment, mechanism of high-speed machining analysis, Finite Element Model (FEM) analysis and coated tool wear, and so on. I have developed a method of preparation of coated tools, and built up high-speed machining experiment system. At the same time, this system is also used to measure cutting force, cutting temperature, cutting vibration, etc. An FEM model of mechanical constitutive relations of materials for high-speed machining has been accomplished, which have been applied to simulate the processing of automotive, mold and aerospace materials. At present, I am undertaking National Natural Science Foundation of China, Natural Science Foundation of Hunan province jointly fund and so on. I have published 65 academic papers and authorized 4 patents

PUBLIC INTEREST STATEMENT

In recent years, conventional machining methods has been gradually replaced by high-speed machining as it is difficult to meet the requirements of the high-quality requirements of components, including shape precision, dimensional accuracy, surface finish and surface integrity. It is well known that hardened steel is widely used to produce many kinds of cold work dies because of its excellent mechanical properties. This article describes some of cutting parameters effects of chip formation, cutting temperature, stress and cutting force, which was used to illustrate impacts of cutter life and surface quality. It was found that optimized cutting parameters can improve the surface integrity of the workpiece and eliminate the residual stress.Clearly, the combination of simulation and experiment have a profound effect on optimization of process parameters of difficult-to-machine material. Understanding these effects can improve the design of cutting inserts in finish milling of hardened steel SKD11 and optimize process parameters.

Subjects: Manufacturing & Processing; Manufacturing Technology; Computer Aided Design & Manufacturing; Materials Processing; Manufacturing Engineering; Automotive Technology & Engineering

Keywords: Finite element simulation; high-speed finish milling; cutting speed; cutting depth; tool-tip radius; hardened steel SKD11

1. Introduction

SKD11 hardened steel is a representative of high carbon and high alloy steels. It has high strength, good heat resistance, good toughness, high hardness and good wear resistance (Koshy, Dewes, & Aspinwall, 2002), SKD11 hardened steel is widely used to produce many kinds of cold work dies, such as blanking punching die and trimming die, cold extrusion die, bending die, drawing die, etc. High-speed milling (HSM) as a kind of metal processing is often regarded as the main processing method of aerospace and automotive industries, because it is able to a certain extent, reduce the workpiece material costs, increase productivity, reduce processing costs and shorten delivery time. Compared to the traditional processing route, in annealing, heat treatment, grinding and electrical discharge machining (EDM), more needs to be introduced. At the same time, the service life of the parts can be improved by improving the surface quality and the processing surface integrity (Kim, Lee, Kang, & Kim, 2001).

In order to make the HSM processing to achieve the same effect as the grinding, high-speed machining should also have the ability to meet the requirements of parts with high quality, including shape precision, dimensional accuracy, surface finish and surface integrity. However, HSM with the traditional cutting machining the difference is that when the spindle speed of 10,000 r/min, due to the cutting depth is relatively small (less than 0.1 mm), before the chip formation occurs only within the tool-tip radius. High-speed finish milling is often regarded as a stable cutting process to obtain satisfied machining precision (Hamdan, Sarhan, & Hamdi, 2012). Due to the inherent complexity of metal cutting technology, finite element method (FEM) has been widely used in the simulation and research of metal cutting process, and these experiments or theoretical analysis methods is difficult to realize or cannot be achieved. Shet and Deng proposed a finite element model to analyze chip formation, stress and strain from an orthogonal cutting of AISI 4341 steel (Shet & Deng, 2003). The friction interaction between the interface of the knife and the chip is analyzed by modified Coulomb friction law. The separation technique of the cutting is simulated by the node release technique based on the critical stress criterion. Outeiro and Umbrello utilizes the commercial finite element analysis (FEA) software DEFORM-2D and experimental method to study the distribution of residual stress induced by orthogonal cutting of AISI 316L steel (Umbrello, Outeiro, & M'Saoubi et al., 2010). Mohamed and Ng proposed an Arbitrary–Lagrangian–Eulerian (ALE) FE approach, which can estimate the effects of cutting edge radius on the residual stresses during the orthogonal dry cutting of austenitic stainless AISI 316L (Nasr, Ng, & Elbestawi, 2007). Nurul et al. found out cutting temperatures is up to 700°C in the process of machining D2 hardened steel, which are largely used to account for the poor tool life by FEM (Hashmi, Yilbas, & Naher, 2010). Axinte and Dewes studied tool wear and workpiece surface integrity in machining H13 at a hardness of 52 HRC using PCBN tools by the method of experimental investigations and empirical modeling (Axinte & Dewes, 2010). Yan et al. researched on cutting force and temperature distribution in the process of cutting, this paper proposes a with ABAQUS/explicit coupled thermal and mechanical model based on the hardening thermal mold AISI H13 (Rockwell hardness of 52) orthogonal milling experiments (Yan, Hua, & Shivpuri, 2005). Ng and Aspinwal employed FORGE 2 to simulate cutting forces and temperature distributions for an orthogonal milling a hardened hot work die steel AISI H13 (Rockwell hardness of 52) and analyzed the continuous and segmental chip formation when machining AISI H13 tool/die steel (Ng & Aspinwall, 2002). However, in the former FEM model, the effect of the initial workpiece hardness on its flow stress is not considered, and the tool is assumed to be very sharp in the latter model, thus limiting their utility, which restricted their utility (Hua & Shivpuri, 2004; Shih, 1996). Therefore, in order to better understand the process, improve the performance of the cutting tool, this study

tries to ignore the factors in the finite element model into some numerical simulations, and the model is used to study the influence of processing parameters on the properties of high-speed steel quenching processing precision milling SKD11.

However, few studies have been performed on materials flow stress which was not adequately described the strain rate hardening effect and the impact of high temperature softening. In this paper, the Split-Hopkinson pressure bar (SHPB) test, analysis of the large strain, strain rate and temperature of the workpiece, and studied the processing parameters in the process of milling hardened steel SKD11 processing performance. The analysis describes the basic mechanics of the main shear zone of strain, strain rate, stress and temperature field.

2. Finite element model

With the development of commercial finite element (FE) software DEFORM-2DTM, a Lagrangian implicit code is chosen to simulate the HSM process of hardened SKD11 steel (Rockwell hardness of 62), while the depth of cut is more than 5 times the feed direction in the process of HSM, this process can be regarded as simplified 2-D cutting process. The thermomechanical coupling implicit finite element model consists of a workpiece and a tool for simulating the 2-D cutting process, as shown in Figure 1 (Tang, Wang, Hu, & Song, 2009). A Lagrangian-Eulerian (ALE) equation with arbitrarily adaptive mesh technique and automatically generated boundaries is utilized to improve the quality and the accuracy of the predicted results. DEFORM-2DTM has the function of dealing with improvement and optimization of HSM processes, and it is possible to optimize cutting parameters and prolong the life-time of cutting tools by reducing cutting forces and cutting temperature without experimental set-up of the processes.

The workpiece (length*width = 3mm*1mm) is initially meshed and subdivided into 8000 isoparametric quadrilateral elements. At the same time, the TiSiN-coated carbide tool with a radius of 20 μm is considered to be rigid and meshing with 700 elements due to its high modulus of elasticity. The cutting conditions and tool geometries (for the simulation and experimental) of high speed finish milling operation can be found in Table 1. And physical properties of SKD11 hardened steel and TiSiN coated cemented carbide tool is shown in Table 2.

The modified constitutive equation of SKD11 hardened steel based on SHPB experimental in HSM operate has been developed, which can be represented by the follow formula (Tang, Wang, Hu, & Song, 2010):

$$\begin{cases} \bar{\sigma} = \left[A + B(\bar{\varepsilon})^n\right]\left(1 + C\ln\frac{\dot{\bar{\varepsilon}}}{\dot{\varepsilon}_0}\right)\left(\frac{\dot{\bar{\varepsilon}}}{\dot{\varepsilon}_0}\right)^k\left[1 - \left(\frac{T - T_0}{T_{melt} - T_0}\right)^m\right] & \text{for T} < \text{Tc} \\ \bar{\sigma} = \left[A + B(\bar{\varepsilon})^n\right]\left(1 + C\ln\frac{\dot{\bar{\varepsilon}}}{\dot{\varepsilon}_0}\right)\left(\frac{\dot{\bar{\varepsilon}}}{\dot{\varepsilon}_0}\right)^k\left[1 - \left(\frac{T - T_0}{T_{melt} - T_0}\right)^m\right]\frac{(\sigma_f)_{def}}{(\sigma_f)_{rec}} & \text{for T} > \text{Tc} \end{cases} \quad (1)$$

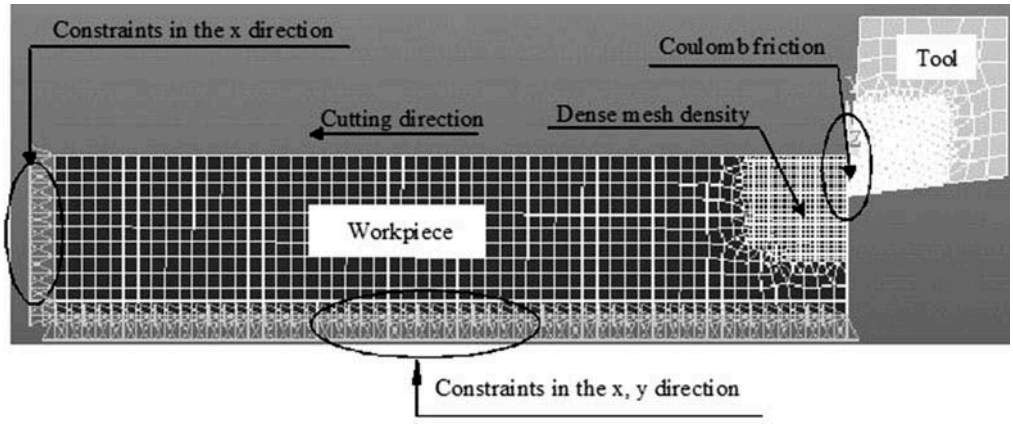

Figure 1. Finite element model of high speed simplified milling of hardened SKD11steel.

Table 1. The cutting conditions and tool geometries in high-speed finish milling

	Workpiece	Tool
Material	SKD11 hardened steel	TiSiN coated cemented carbide
Object type	Rigid–plastic	Rigid
Young's modulus (GPa)	210	473.8
Poisson's ratio	0.28	0.22
Density (kg/m^3)	7950	11,900
Thermal conductivity (W/m °C)	47.44 − 0.0298T	35.95 + 0.042T
Specific heat (J/kg °C)	447 + 0.504T	334.01 + 0.12T

Table 2. Physical properties of SKD11 hardened steel and TiSiN coated cemented carbide

A(MPa)	B(MPa)	n	C	m	K	$(\sigma_f)_{rec}$	$(\sigma_f)_{def}$
2480	1440	0.45	0.012	1.1	−0.01	1560.9765	800.0941

Table 3. The parameters of the Johnson-Cook constitutive equation of hardened SKD11 steel (Tang et al., 2010)

Tool rake angle (°)	5
Tool clearance angle (°)	10
Tool-tip radius (um)	10, 20, 40
Cutting speed (m/min)	100, 300,700
Depth of cut (um)	5, 10, 20

where $\bar{\sigma}$ is the flow stress, $\bar{\varepsilon}$ is the plastic strain, $\dot{\bar{\varepsilon}}$ is the strain rate (s), $\dot{\varepsilon}_0$ is the reference plastic strain rate (s^{-1}), T (°C) is the workpiece temperature, T_{melt} is the melting temperature of the workpiece material and T_0 (20°C) is the room temperature, T_c is the recrystallization temperature, $(\sigma_f)_{rec}$ and $(\sigma_f)_{def}$ are the flow stresses just prior to and after the recrystallization, respectively. The material yield strength is defined as coefficient A (MPa), the hardening modulus is defined as coefficient B (MPa) and the strain rate sensitivity coefficient is defined as coefficient C, while the m, n coefficients relate to workpiece material hardness. The hardening coefficient and the thermal softening coefficients are defined separately as coefficient n and m. Their values are taken from Ref (Tang et al., 2010) as shown in Table 3.

The friction coefficient, obtained by using a Coulomb model, is shown to be closer to the true model (Tang et al., 2009). Cockroft and Latham's criteria are used to predict the effect of tensile stress on chip segmentation during orthogonal cutting. The value 0.22 is selected as SKD11 hardened steel material constant. Residual stresses induced by phase transformation and cutting tool wear are not taken into. In addition, the initial residual stress is not taken into as before the first cut should be zero.

3. Heat transfer model

This rigid-plastic material model is employed with a heat transfer model (the heat exchange cornering the workpiece, cutting tool, chip and ambient surrounding). The function of the heat flow process is given as:

$$\lambda\left(\frac{\partial^2 T}{\partial x^2}+\frac{\partial^2 T}{\partial y^2}\right)+Q=\rho C_p\left(\mu_x\frac{\partial T}{\partial x}+\mu_y\frac{\partial T}{\partial y}\right) \tag{2}$$

where λ is thermal conductivity, T represents the tool temperature, ρ is density of the material, Cp is the specific heat and Q should satisfy the equation:

$$Q = \bar{\sigma}\dot{\bar{\varepsilon}}/J \tag{3}$$

where J is the mechanical equivalent of heat, $\bar{\sigma}$ is flow stress, and $\dot{\bar{\varepsilon}}$ is strain rate. And its boundary conditions are as follow:

$$T_0 = 20^{\circ}\mathrm{C} \tag{4}$$

$$-k\frac{\partial T}{\partial n} = h_c(T - T_0) \tag{5}$$

Here h_c is the convection heat transfer coefficient, T_0 is the ambient temperature, for example taken as 20°C.

4. Chip separation criteria and friction model

In the process of high speed cutting, Cockroft and Latham's criterion is usually used to predict the effect of tensile stress on the chip segmentation (Hua & Shivpuri, 2004). The Cockroft and Latham's criterion can be expressed as:

$$\int_0^{\bar{\varepsilon}_f} \sigma_1 d\bar{\varepsilon} = C \tag{6}$$

where ε_f is the effective strain, σ_1 is the maximum stress and C is a material constant. When SKD11 hardened steel material constant C is up to 0.22, the fracture occurs or chip segmentation starts, and the disabled elements will be removed from the calculation circle (Tang et al., 2009).

The first zone is named as the sticking zone, where the normal stress is very large and the frictional stress is equal to the shear stress of the machined material. However (or in contrary), the normal pressure in the latter region is smaller, Coulomb theory can provide a feasible model for the interpretation of the phenomenon. This can be expressed by the following:

$$\tau_f = \mu\sigma_n \text{ for } \tau_f < k \tag{7}$$

$$\tau_f = k \text{ for } \tau_f \geq k \tag{8}$$

where τ_f is the frictional stress; σ_n is the normal stress; and μ is coefficient of friction, which is parameterized as 0.6, 0.4 and 0.2 in cutting speeds of 100 m/min, 300 m/min and 700 m/min, respectively; k is the shear flow stress of the working material.

5. FEM simulation analysis

5.1. Effect of the cutting speed

The effect of cutting speed was studied setting the parameters as: depth of cut = 10 um, rake angle = 5°, clearance angle = 10°and tool-tip radius = 20 μm. Figure 2 shows the chip geometries at the three different speeds. It should be it can be seen from Figure 2, with the increase of cutting speed, the sawtooth shape of the chip is becoming more and more obvious. The conversion from continuous chip to segmented chip is improved at a cutting speed of 100 to 700 m/min. The similar observation was presented by Tang et al. (Tang et al., 2009). Figure 3 illustrates the distributions of effective stresses at three different cutting speeds. The effective stress distribution in the cutting deformation zone is similar to that of the three different cutting speeds, but the cutting speed has a greater influence on the cutting deformation. When cutting speed is up to 700m/min, the effective stress is mainly concentrated in the shear deformation area. The maximum tensile effective stress decreases in machined layer with increasing cutting speed. Therefore, it is useful to appropriately increase the cutting speed by cutting. Figure 4 shows the temperature distribution at three different cutting speeds. The magnitude and distribution of the temperature is affected by

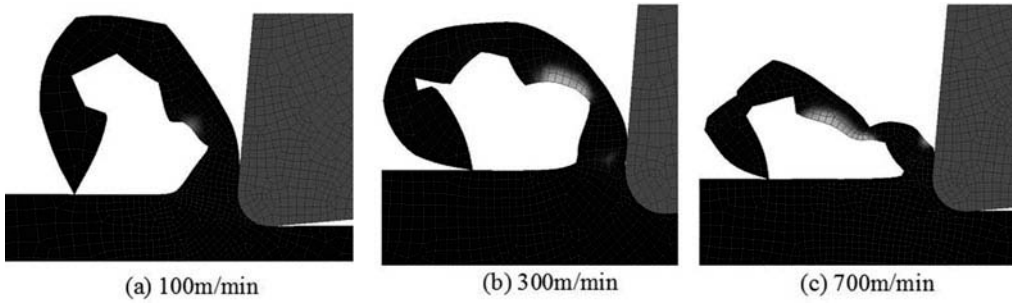

Figure 2. Chip formations in three different cutting speeds.

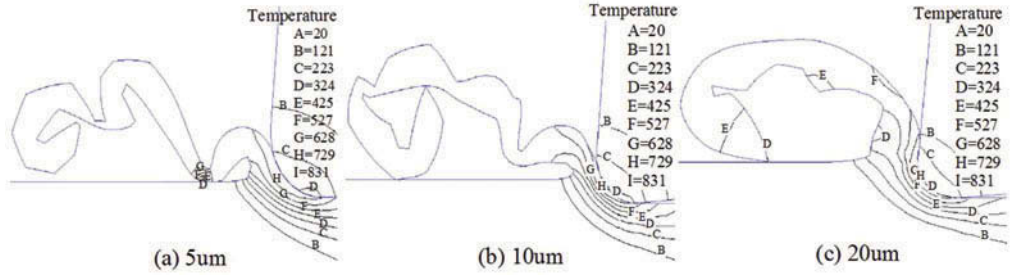

Figure 3. Effective stress distributions in three different cutting speeds (Unit: MPa).

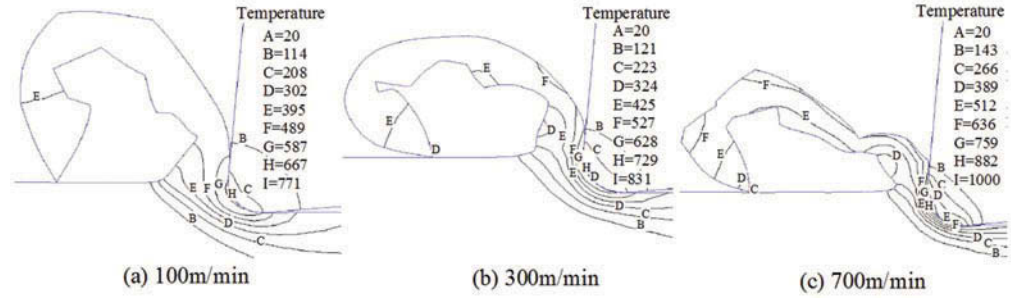

Figure 4. Cutting temperature distributions in three different cutting speeds (Unit:°C).

the cutting speed. Indicating that the maximum workpiece temperature increased from 632°C to 948°C, the maximum temperature of the tool increased from 228°C to 347°C, cutting speed from 100 m/min to 700 m/min. With the increase of cutting speed, the high temperature areas are concentrated on the chip–tool interface.

5.2. Effect of the cutting depth

The effect of cutting depth was analyzed setting the parameters as: cutting speed = 700 m/min, rake angle = 5°, clearance angle = 10°and tool-tip radius = 20 μm. Figure 5 represents the chip geometries at three different cutting depths. It should be it can be seen from Figure 5, with the increase of cutting depth, the ability of chip deformation decreases. When cutting depth is 10 um, the shear deformation is the most severe. Figure 6 shows the distributions of effective stresses at three different cutting depths. As the increases of cutting depth, the effective stress increases as well, and the maximum effective is up to 2698MPa. Figure 7 is the distributions of temperatures at three different cutting depths. The cutting temperature is almost impervious to the depth of cutting, in the process of high-speed finish milling. The maximum workpiece temperature always changes between 778 and 801°C, while the maximum tool temperature increases from 276 to 316°C when the cutting depth is increased from 10 to 40 μm.

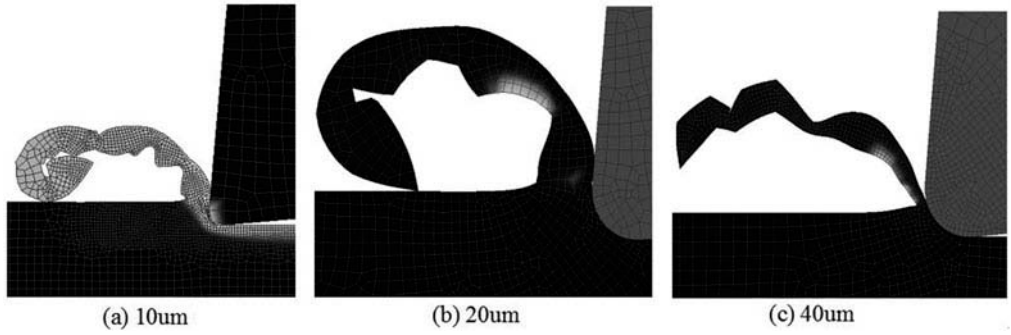

Figure 5. Chip formations in three different depths of cut.

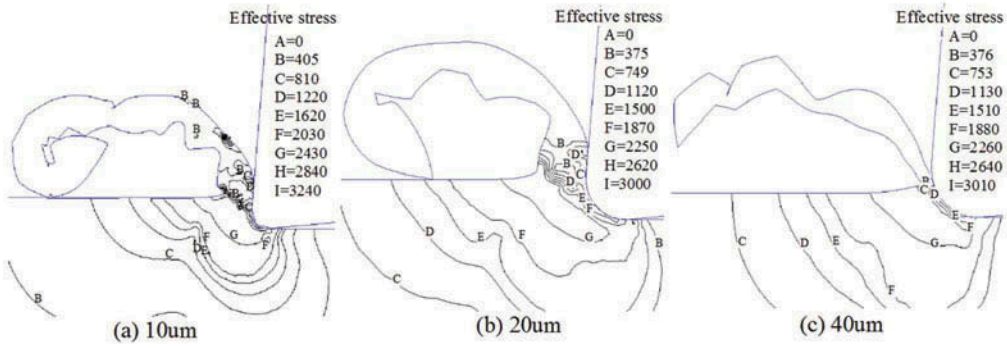

Figure 6. Effective stress distributions in three different depths of cut (Unit: MPa).

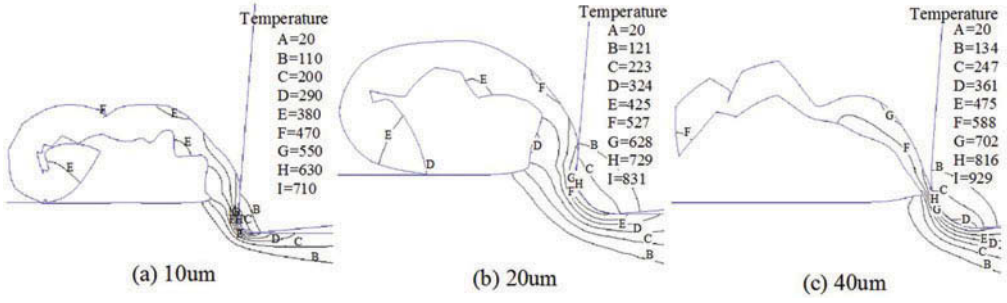

Figure 7. Cutting temperature distributions in three different depths of cut (Unit:°C).

5.3. Effect of the tool-tip radius

The parameters for the study of effects of the tool-tip radius are: cutting depth of 10 μm, cutting speed = 700 m/min, rake angle = 5°, clearance angle = 10°and tool-tip radius = 20 μm. Figure 8 illustrates the chip geometries at three different tool-tip radius. It can be seen from Figure 8, when the tool-tip radius is 10 um, the deformation degree of saw-tool chip is very obvious. Figure 9 represents the distribution of effective stresses at three different tool-tip radius. When the tool-tip radius increases from 5μm to 20μm, the maximum tensile effective stress increases from 2778 to close to 2980 MPa. These predictions help to understand the function of selecting the appropriate tool nose radius in high-speed finishing operations. Figure 10 shows the temperature distributions of at three different tool-tip radius. The largest workpiece temperature increased from 687 to about 812°C, its mainly concentrated in the shear deformation zone. When the maximum temperature of the tool increases from 258 to 331, the cutter radius increases from 20 to 40um.

6. Compare of experimental cutting force and simulation results in finish milliing

Mitsubishi M70 digital controller for cutting force test is carried out by the use of high-speed machining center JC-30. The maximum machine spindle speed is 24,000 rpm. An SKD11 hardened steel (Rockwell

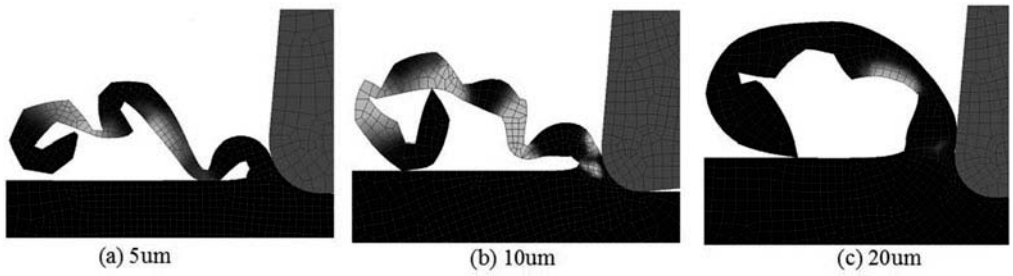

Figure 8. Chip formations in three different tool-tip radius.

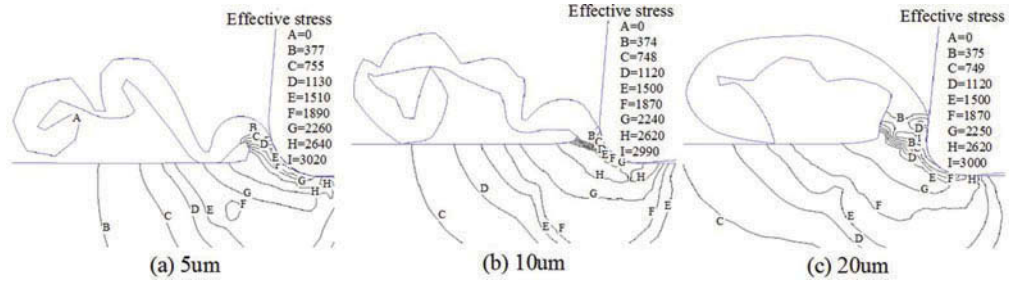

Figure 9. Effective stress distributions in three different tool-tip radius (Unit: MPa).

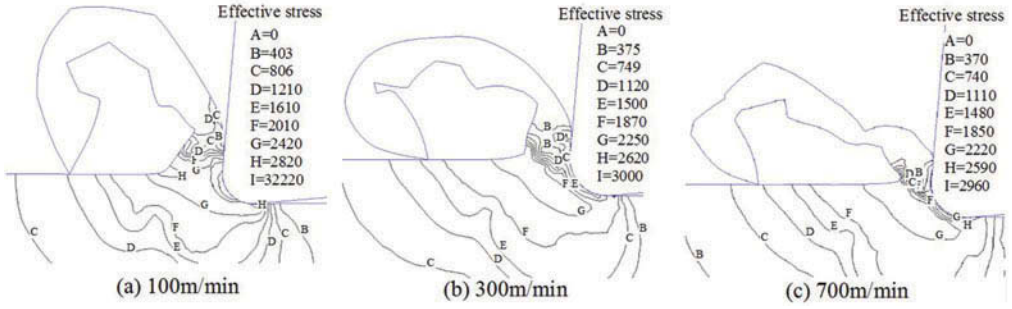

Figure 10. Cutting temperature distributions in three different tool-tip radius (Unit:°C).

hardness of 62) with a thickness of 30 mm was mounted on a three-component piezoelectric dynamometer (Kistler type 9272), which was connected with charge amplifier (Kistler type 5070)) and a personal computer data acquisition system. The cutting forces analyzed in this paper are the average cutting forces in the *X* and *Y* directions, including F_x and F_y. The workpiece material used was hardened mold steel (Rockwell hardness of 62); its main chemical ingredients are: C 1.40–1.60, Si ≤ 0.40, Mn ≤ 0.60, P ≤ 0.030, S ≤ 0.030, Cr 11.00–13.00, Mo 0.80–1.20, Ni≤ 0.50, V 0.20–0.50, Cu≤ 0.25. The cutting tool material is TiSiN-coated cemented carbide.

In order to analyze the high-speed finishing process, the cutting and feeding forces can be calculated by the finishing process, with each cutting depth incremented at each angle of the tool rotation. The measured forces in the *X* and *Y* directions, F_x and F_y, can be resolved at each tool rotation angle φ in the cutting and the feed directions can be expressed as:

$$\begin{cases} F_t = F_y \sin\varphi - F_x \cos\varphi \\ F_c = F_x \sin\varphi + F_y \cos\varphi \end{cases} \tag{9}$$

According to equation (22), it was possible to calculate the force during high-speed finish cutting. Therefore, the obtained results were compared with the predicted values from the simulations. The deviation errors between experimental and simulation results were concluded using the following formula (23), and the errors can be found in Table 4.

Table 4. Comparison of experimental cutting force and simulation result in different cutting parameter

Cutting parameter	Parameter values	$\bar{F}x$(N)			$\bar{F}y$(N)		
		Predicted (FEM)	Measured	Error	Predicted (FEM)	Measured	Error
Cutting Speed (m/min)	100	118.22	112.86	3.92%	126.23	134.47	6.52%
	300	98.62	106.78	8.27%	131.59	118.65	10.9%
	700	94.12	88.63	6.19%	119.95	108.31	10.7%
Depth of cut (um)	5	48.12	54.72	13.7%	89.89	100.01	11.2%
	10	62.31	70.13	12.5%	96.77	108.54	12.7%
	20	90.76	97.66	7.6%	112.16	122.36	9.1%
Tool-tip radius (um)	10	82.37	90.11	9.4%	59.49	67.42	13.3%
	20	98.66	106.21	7.6%	114.36	121.84	6.5%
	40	127.56	134.79	5.6%	198.59	205.04	3.2%

$$Error = \frac{Experimental\_value - Simulate\_value}{Experimental\_value} \times 100\% \quad (10)$$

It can be seen that the differences of cutting forces between the predicted cutting forces and the experimental data are within 3.2–13.7%.When the cutting speed is increased, the reduction of the cutting force can be considered as the effect of heat softening. At the same time, it can be seen from the simulation results that this leads to the change of the effective stress-strain curve of the workpiece material, which increases the shear angle, thereby reducing the amount of plastic deformation required to deform the chip.

The F_x and F_y forces in the X and Y directions decrease with increasing cutting speed, this is because segmented chips cause an additional decrease in the cutting force due to energetically favorable. But the thrust force is larger than the cutting force for the higher cutting speed of 700 m/mm; when the depth of the cut increases, the F_x and F_y forces in the X and Y directions also increases, this is due to the increase of cutting thickness in unit area, resulting in increasing cutting force. The F_x and F_y forces in the X and Y directions increase with increasing tool-tip radius, but the F_y forces in the Y directions is larger than the F_x forces in the X directions for three tool-tip radius.

7. Conclusions

In this paper, the effect of cutting speed, cutting depth and tool-tip radius on the chip formation, cutting temperature and effective stress of cutting speed is studied during high speed finish milling of SKD11 hardened steel. It mainly concludes that:

(1) The predicted cutting forces and the experimental data are within 3.2–13.7%. It is shown that a coupled thermo-mechanical implicit finite element model can be used to predict chip formation, cutting temperature and effective stress in high speed finish milling of SKD11 hardened steel.

(2) The simulation results show that higher speed, smaller cutting depth and larger tool-tip radius reduce the effective tension in the working layer, thus improving the surface integrity of the workpiece and eliminating the residual stress. It is also helpful to improve the design of the cutting insert, especially in order to optimize the edge geometry of the TiAlSiN blade for precision machining of hardened steels.

(3) The F_y force in the Y direction is dominant and larger than the cutting force in finish hard machining. As the cutting speed increases, the F_x and F_y forces decrease, which increases the

surface integrity of the machined workpiece. However, F_y force, especially in the *Y* direction, increases as the feed and tip radius increases. It is observed that when the feed and tip radius increases, the high stress region in the thrust direction changes inward, which may result in higher residual stress on the finishing surface and faster flank wear.

Nomenclature

$\bar{\sigma}$ (MPa)	Flow stress
$\bar{\varepsilon}$	Plastic strain
$\dot{\bar{\varepsilon}}$ (s^{-1})	Strain rate
$\dot{\bar{\varepsilon}}_0$ (s^{-1})	Reference strain rate
T (°C)	The workpiece temperature
T_{melt} (°C)	The melting temperature of the workpiece material
T_0 (°C)	The room temperature
Tc (°C)	The recrystallization temperature
$(\sigma_f)_{def}$ (MPa)	The flow stresses after the recrystallization
$(\sigma_f)_{rec}$ (MPa)	Flow stress before crystallization
A (MPa)	The material yield strength
B (MPa)	The hardening modulus
C	The strain rate sensitivity coefficient
m	Material softening exponent
n	Pressure hardening exponent
λ (w/m)	Thermal conductivity
ρ (Kg/m^3)	Material density
Q (J)	Heat
C_p (J/Kg)	The specific heat
J (J)	The mechanical equivalent of heat
H_c	The convection heat transfer coefficient
ε_f	The effective strain
σ_1 (MPa)	The maximum stress
τ_f	The frictional stress
σ_n (MPa)	The normal stress
u	Coefficient of friction
k (MPa)	The shear flow stress of the working material
F_x (N)	Cutting force in x direction
F_y (N)	Cutting force in y direction
F_t (N)	Cutting force in the tangential direction
F_c (N)	Cutting force in the radial direction
Ø (°)	Tool rotation angle
HSM	High-speed milling
HRC	Rockwell hardness
FEM	Finite element method

Acknowledgements
The authors gratefully acknowledge the funding by the Natural Science Foundation of Hunan Province with the project number 2015JJ5023; Hengyang Industry-University-Research Collaboration project with the project number 2017KJ143; outstanding young scientist project in Hunan province department of education with the project number 15B206.

Funding
This work was supported by the Natural Science Foundation of Hunan Province [2015JJ5023];outstanding young scientist project in Hunan province department of education [15B206];Industry-university-research cooperation project of Hengyang [2017KJ143].

Author details
Tang Dewen[1,2]
E-mail: will998@163.com
Peng Cong[2]
E-mail: 26379198@qq.com
Zhang Jiayu[2]
E-mail: 5633973@qq.com
[1] School of mechanical engineering, University of South China, Hunan, China.
[2] Hunan Provincial Key Laboratory of Emergency Safety Technology and Equipment for Nuclear Facilities, University of South China, Hunan, China.

Citation information
Cite this article as: Finite element simulation of high-speed finish milling of SKD11 hardened steel based on modified constitutive equation, Tang Dewen, Peng Cong & Zhang Jiayu, *Cogent Engineering* (2018), 5: 1482589.

References

Axinte, D., & Dewes, R. (2010). High-speed milling of AISI H13 hot-work tool steel using polycrystalline cubic boron nitride ball-nose mills: From experimental investigations and empirical modelling to functional testing of the machined surfaces. *Proceedings of the Institution of Mechanical Engineers, Part B: Journal of Engineering Manufacture*, *224*(1), 15–24. doi:10.1243/09544054JEM1630

Hamdan, A., Sarhan, A. A. D., & Hamdi, M. (2012). An optimization method of the machining parameters in high-speed machining of stainless steel using coated carbide tool for best surface finish. *The International Journal of Advanced Manufacturing Technology*, *58* (1–4), 81–91. doi:10.1007/s00170-011-3392-5

Hashmi, M. S. J., Yilbas, B. S., & Naher, S. (2010). Prediction of tool life and experimental investigation during hot milling of Aisi H13 tool steel. *Advanced Materials Research, 2010*(83-86), 190-197. Retrieved from.https://doi.org/10.4028/www.scientific.net/AMR.83-86.190

Hua, J., & Shivpuri, R. (2004). Prediction of chip morphology and segmentation during the machining of titanium alloys. *Journal of Materials Processing Technology*, *150*, 124–133. doi:10.1016/j.jmatprotec.2004.01.028

Kim, S. W., Lee, D. W., Kang, M. C., & Kim, J. S. (2001). Evaluation of machinability by cutting environments in high-speed milling of difficult-to-cut materials. *Journal of Materials Processing Technology*, *111*(1), 256–260. doi:10.1016/S0924-0136(01)00529-5

Koshy, P., Dewes, R. C., & Aspinwall, D. K. (2002). High speed end milling of hardened AISI D2 tool steel (□58 HRC). *Journal of Materials Processing Technology*, *127*(2), 266–273. doi:10.1016/S0924-0136(02)00155-3

Nasr, M. N. A., Ng, E. G., & Elbestawi, M. A. (2007). Modelling the effects of tool-edge radius on residual stresses when orthogonal cutting AISI 316L. *International Journal of Machine Tools and Manufacture*, *47*(2), 401–411. doi:10.1016/j.ijmachtools.2006.03.004

Ng, E. G., & Aspinwall, D. K. (2002). Modelling of hard part machining. *Journal of Materials Processing Technology*, *127*(2), 222–229. doi:10.1016/S0924-0136(02)00146-2

Shet, C., & Deng, X. (2003). Residual stresses and strains in orthogonal metal cutting. *International Journal of Machine Tools and Manufacture*, *43*(6), 573–587. doi:10.1016/S0890-6955(03)00018-X

Shih, A. J. (1996). Finite element analysis of orthogonal metal cutting mechanics. *International Journal of Machine Tools and Manufacture*, *36*, 255–273. doi:10.1016/0890-6955(95)98765-Y

Tang, D. W., Wang, C. Y., Hu, Y. N., & Song, Y. X. (2009). Finite-element simulation of conventional and high-speed peripheral milling of hardened mold steel. *Metallurgical and Materials Transactions A*, *40*(13), 3245–3257. doi:10.1007/s11661-009-9983-1

Tang, D. W., Wang, C. Y., Hu, Y. N., & Song, Y. X. (2010, April). Constitutive equation for hardened SKD11 steel at high temperature and high strain rate using the SHPB technique. In *Fourth International Conference on Experimental Mechanics* (Vol. 7522, 6B-75226B-12). International Society for Optics and Photonics.

Umbrello, D., Outeiro, J. C., M'Saoubi, R., JayaldI, A. D., & Jawahir. I. S. (2010). A numerical model incorporating the microstructure alteration for predicting residual stresses in hard machining of AISI 52100 steel. *CIRP Annals-Manufacturing Technology*, *59*(1), 113–116. doi:10.1016/j.cirp.2010.03.061

Yan, H., Hua, J., & Shivpuri, R. (2005). Numerical simulation of finish hard turning for AISI H13 die steel. *Science and Technology of Advanced Materials*, *6*(5), 540–547. doi:10.1016/j.stam.2005.04.002

Cogent Engineering **(ISSN: 2331-1916) is published by Cogent OA, part of Taylor & Francis Group.**

Publishing with Cogent OA ensures:

- Immediate, universal access to your article on publication
- High visibility and discoverability via the Cogent OA website as well as Taylor & Francis Online
- Download and citation statistics for your article
- Rapid online publication
- Input from, and dialog with, expert editors and editorial boards
- Retention of full copyright of your article
- Guaranteed legacy preservation of your article
- Discounts and waivers for authors in developing regions

Submit your manuscript to a Cogent OA journal at www.CogentOA.com